Linker Deficiency, Aromatic Ring Fusion and Electrocatalysis in a Porous Ni_8 Pyrazolate Network

Jieying Hu[†], Xiangling Deng [†], Hu Zhang[†], Yingxue Diao[‡], Shengxian Cheng[‡], Sai-Li Zheng[†], Wei-Ming Liao[†], Jun He[†,*], Zhengtao Xu[‡,*]

[†]*School of Chemical Engineering and Light Industry, Guangdong University of Technology, Guangzhou, 510006, Guangdong, P. R. China*

[‡]*Department of Chemistry, City University of Hong Kong, 83 Tat Chee Avenue, Kowloon, Hong Kong, P. R. China*

The cruciform linker molecule here features two designer functions: the pyrazole donors for framework construction, and the vicinal alkynyl units for benzannulation to form nanographene units into the Ni_8-pyrazolate scaffold. Unlike the full 12 connections of the $Ni_8(OH)_4(H_2O)_2$ clusters in other Ni_8-pyrazolate networks, significant linker deficiency was observed here, leaving about half of the Ni(II) sites capped by acetate ligands, which can be potentially removed to open the metal sites for reactivity. The crystalline Ni_8-pyrazolate scaffold also retains the crystalline order even after thermal treatments (up to 300 °C) that served to partially graphitizes the neighboring alkyne units. The resultant nanographene components enhance the electroactive properties of the porous hosts, achieving hydrogen evolution reaction (HER) activity that rivals topical nickel/palladium-enabled materials.

Recently, we have studied cascade cyclization of alkyne units built into the linker molecules of metal-organic frameworks (e.g., the relatively stable Zr^{4+}-carboxyl systems).[1-3] The thermally triggered cyclization (e.g., above 300 °C) leads to cross-linked, partially graphitized products that feature enhanced polarizability (e.g., black in color) and chemical stability. Topically, this line of work bears on the endeavors to assemble polarizable, large-π molecules into MOF scaffold to enhance photophysical and electronic properties[4-16]. The two-step (i.e., crystallization-cyclization) approach, however, serves two important purposes. First, it utilizes open-arm alkyne precursors to avoid the solubility problems caused by the tight-packing large-π aromatics. Second, the extensive crosslinking and merging of the linker molecules transforms the coordination precursor into a covalent framework. Conceptually this work can also be considered a leap into the infinite network from the intramolecular ring closures reported by Hupp, Stoddart and Farha,[17,18] and more recently by Zhou.[7]

The Zr(IV)-carboxylate coordination links are, however, highly ionic, and often exhibits structural lability leading to contraction or partial collapse of the host framework (e.g., when the solvent molecules are evacuated)[1,19-23]. Such structural lability hampers the thermocyclization studies, because it can degrade the structural order of coordination scaffold and that of the thermocyclized product, thereby

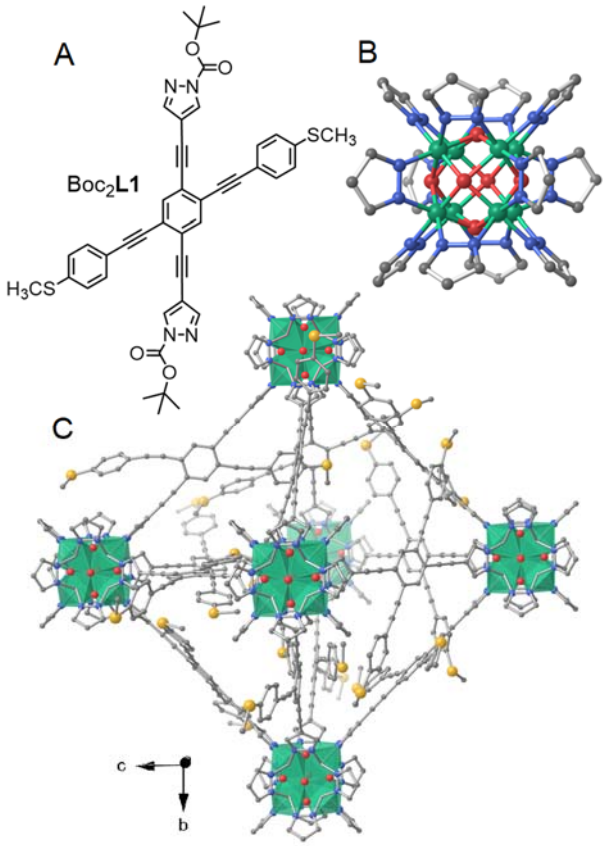

Figure 1. a) The cruciform molecule Boc_2**L1** (featuring four alkyne arms); b) A $Ni_8(OH)_4(H_2O)_2$ (abbreviated as Ni_8O_6) cluster with 12 associated pyrazolate units; c) view of an octahedral unit in an idealized model (i.e., assuming full linker occupancy) of the **fcu** net of Ni**L1** along the *a* axe. H atoms were omitted for clarity. Red spheres, O; grey, C; blue, N; green, Ni-based polyhedral.

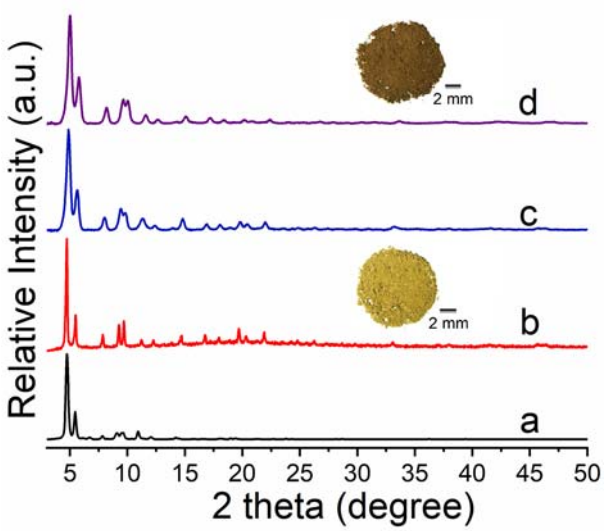

Figure 2. PXRD patterns (Cu Kα, λ = 1.5418 Å) for Ni**L1**: (a) calculated from the crystal structure model following **fcu** topology; (b) measured from an as-made sample (Inset: a photograph of an as-made sample of Ni**L1**); (c) from an activated sample; (d) from an as-made sample heated at 300 °C for 2h, i.e., Ni**L1**-300**,** (Inset: a photograph of Ni**L1**-300).

complicating characterization. The framework contraction/collapse can also significantly reduce the accessible surface area in the solid state, and limit the use as porous materials.

In this connection, the more robust Ni_8-pyrazolate nets[24-28] are of interest. These consist of the secondary building unit of a Ni_8 cube with its six faces occupied by OH^- or H_2O species, and its 12 edges paralleled by the N-N units of the pyrazolate ligands, each of which straddles two Ni centers. The 12-connected Ni_8O_6 node can be considered topologically equivalent to the $Zr_6O_4(OH)_4^{12+}$ unit (e.g., as in the UiO series), which features a Zr_6 octahedron and an O^{2-} or OH^- species on its 8 faces. One difference, however, is noted: while Ni_8-pyrazolate nets reported so far uniformly feature full linker occupancy (i.e., one Ni_8O_6 node per six ditopic linker to give the 12 connections), the $Zr_6O_4(OH)_4$ unit was often found to fall short of the full 12 connections[21,29-31], e.g., with the missing linkers filled in by monotopic formate/acetate or OH^-/H_2O ligands. Another difference lies in the softer Ni(II)-pyrazolate pair (relative to Zr^{4+}-carboxylate), which imparts more covalency and stability to the bonding, making the resulted framework less prone to deformation and degradation. In the context of the thermocyclized carbon framework, the more active Ni centers can be useful for catalysis; and the pyrazolate-Ni bonds also feature closer orbital overlap and electronic coupling to promote, for example, electrocatalytic performance.

To implement cascade cyclization in the Ni_8-pyrazolate system, we design the cruciform molecule **L1**, which features two pyrazolate units in a linear array, and two pairs of contiguous alkynyl units on the central benzenoid ring for cyclization in the prospective MOF scaffold. As a handle for functionalization, we also attached the thioether donors to the two side arms. We will describe the porous cubic Ni_8O_6-**L1** framework product (denoted as Ni**L1**), which maintains the crystalline order even when heated to 300 °C for effecting the cyclization of the vicinal alkyne units. The thermally induced partial graphitization expands the polycyclic conjugated system throughout the solid state, and enhances electroactivity as is reflected in the hydrogen evolution reaction studies. Also noted is the discovery of substantial linker deficiency in Ni_8O_6-**L1**, leaving a significant fraction of the Ni(II) sites as potentially open metal sites[32,33] for functional uses (e.g., as Lewis acids).

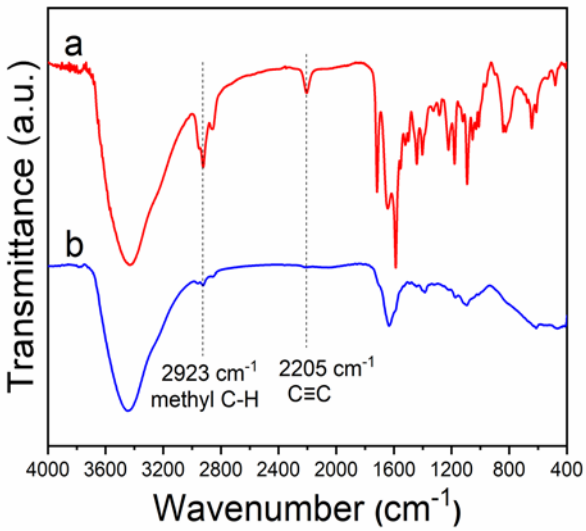

Figure 3. The FT-IR spectra for samples of (a) activated Ni**L1**; (b) Ni**L1**-300.

The yellow, crystalline powder of Ni**L1** (see Figure 2 for a photograph of the as-made sample of Ni**L1**) was solvothermally prepared from molecule Boc_2**L1** (Figure 1A) and $Ni(OAc)_2{\cdot}4H_2O$ (e.g., with **L1**/Ni ratio = 1:2), using *N,N*-dimethylacetamide and H_2O as solvent (water also helps deprotect the *t*-butyl dicarbonate). The *t*-butoxycarbonyl group (BOC) masks the pyrazol donors and reduces their interference in the Sonogashira coupling reaction; the solubilizing BOC group also makes for easier purification, and its *in situ* demasking in the solvothermal synthesis promotes product's crystallinity. Powder X-ray diffraction (PXRD) reveals a cubic lattice (a = 32.366 Å; Figure 2b; details of refinement are included in the ESI). A crystal structure can be modeled based on the secondary building block of $[Ni_8(OH)_4(H_2O)_2]$ (Figure 1B), and the resultant network is isoreticular to a Ni(II)-MOF reported by the groups of Bordiga[34], Galli[24] and Li[35] which features the **fcu** topology (with an fcc array of the Ni_8 clusters).

Elemental analysis found C (47.73%), H (3.70%), N (6.17%) and S (6.83%) for an activated sample of Ni**L1**, with a fitting formula determined to be $Ni_8(OH)_4(H_2O)_2$(**L1**)$_3(CH_3COO)_6(H_2O)_{15}$, which gives a calculated profile of C (48.14%), H (4.11%), N (5.91%)] and S (6.76%)]. The presence of the acetate (CH_3COO^-) component is also verified by dissolving the solid sample in DCl/D_2O for solution NMR measurement (Figure S2). Compared with the formula $Ni_8(OH)_4(H_2O)_2$(**L1**)$_6$ dictated by the idealized **fcu** net, in which the Ni_8 cluster is connected to 12 pyrazolate units (as proffered by the 6 ditopic **L1** linkers), the determined formula

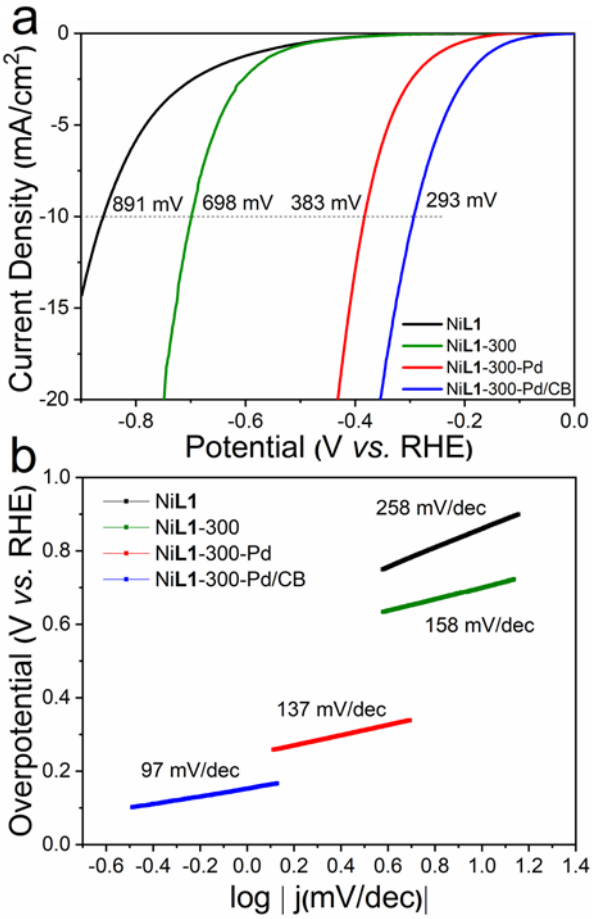

Figure 4. a) Linear sweep voltammetry (LSV) curves of HER for Ni**L1**, Ni**L1**-300, Ni**L1**-300-Pd and Ni**L1**-300-Pd/CB samples dispersed on GCE in N_2-saturated 0.5 M H_2SO_4 electrolyte; b) Tafel plots derived from HER polarization curves in a).

indicates that about half of the **L1** sites are vacant (e.g., replaced by CH_3COO^-) in the current sample. Comparably, motifs of Ni-O clusters featuring mixed carboxyl/pyrazolate ligands are known.[34,36] Thermogravimetric analysis (TGA; conducted in air; Figure S3) reveals a steep weight loss of about 60% between 310 and 410 °C, which can be ascribed to linker decomposition. PXRD on the residue feature distinctly the NiO phase (Figure S4). The residual weight found (25.4 wt%) is slightly higher than the NiO fraction (23.2%) in $Ni_8(OH)_4(H_2O)_2(\mathbf{L1})_3(CH_3COO)_6$: the difference can be accounted for by some amorphous constituent, e.g., as revealed by the diffuse hump at 2θ = 25° in the PXRD pattern of Figure S4. The linker deficiency in Ni**L1** is likely due to the steric interference from the long and rigid alkyne side arms, which make it harder to fit the bulky linkers around the Ni_8O_6 cluster.

The as-made Ni**L1** solid was heated under an argon flow (e.g., 109 mg; for 2 hours) at various temperatures. PXRD indicates that its crystalline order can withstand up to 300 °C (PXRD pattern d in Figure 2; with the product, ca 89 mg, being denoted as Ni**L1**-300), whereas higher temperatures (e.g., 350 °C; see Figure S5 for the PXRD patterns) results in amorphous products. Unlike the yellow as-made Ni**L1**, Ni**L1**-300 is dark brown (see insets of Figure 2 for the photographs; see Figure S6 for the diffuse reflectance spectra). The IR spectra indicates that the distinct alkyne stretching at 2205 cm^{-1} of Ni**L1** completely disappeared in the thermally treated sample of Ni**L1**-300 (Figure 3). In addition, the C–H peak at 2923 cm^{-1} associated with the CH_3S groups of Ni**L1** was also greatly weakened in Ni**L1**-300, indicating the cleavage of the CH_3–S bond, e.g., to form aryl–S–aryl bonds, and to emit CH_3SCH_3 and other small molecules (see Figure S7 for a proposed reaction scheme).

To further characterize the emitted molecules, a sample of Ni**L1** (activated by Soxhlet extraction at 90 °C with methanol for 24 hours) was heated in a sealed tube at 300 °C for 2 hours, after which $CDCl_3$ was then added into the tube pre-frozen by liquid nitrogen to collect the soluble products for NMR analysis. The ^{1}H NMR spectrum (Figure S8) indicates the formation of CH_3SCH_3, and (methylthio)benzene which can be rationalized as being split from the thermocyclizing linker molecules. Curiously though, the ^{1}H NMR spectrum also features a strong peak for benzene (δ = 7.36), whose origin remains to be further elucidated. As shown in Figure S9, analysis of exhaust by thermogravimetric, gas chromatography and mass spectrometry (TG-GC-MS) coupling also confirms the eluents of CH_3SCH_3, and (methylthio)benzene, as well as benzene.

Ni**L1** and Ni**L1**-300 exhibit comparable stability in boiling water, and in acid and base solutions, as shown by the PXRD patterns in Figure S10. Notably, the crystallinity of both remains intact after immersion in 10 M NaOH for 24 hours. Treatment by 15 M NaOH (for 24 hours) does not affect the crystallinity of the thermocyclized sample of Ni**L1**-300, but degrades that of Ni**L1**, as seen in the weaker peaks in the PXRD pattern. The enhanced base-stability of Ni**L1**-300 can be ascribed to the inter-linker covalent links (e.g., the aryl-S-aryl bonds) formed in the vigorous thermal treatment process. Ni**L1** and Ni**L1**-300 are also stable to HCl solutions of pH = 3, but at pH = 1 some degree of degradation occurs, as observed in the broadened PXRD peaks. Similar acid sensitivity was reported of other Ni_8-pyrazolate frameworks.[25,35,37]

The activated Ni**L1** and Ni**L1**-300 solids are also stable in air and vacuum, and can be conveniently used for gas sorption studies. The N_2 adsorption–desorption isotherms collected at 77 K (Figure S11-14) exhibit typical type-I characteristics, with the corresponding BET surface areas of Ni**L1** and Ni**L1**-300 being 465 m^2/g and 340 m^2/g, respectively. Perhaps, the larger surface area of Ni**L1** here arises from the extended side arms that offer additional contact with the sorbate molecules (whereas in Ni**L1**-300 the side branches are fused with the backbone). The measured pore volume of Ni**L1**-300 is 0.829 cm^3/g, greater than the 0.611 cm^3/g of Ni**L1**, which can also be rationalized by the fact that merging of the side arms empties out more space in the framework matrix. In a preliminary two-probe measurement, the conductivity of and Ni**L1**-300 exhibits a higher conductivity (1.08×10^{-5} S/m) than Ni**L1** (7.94×10^{-7} S/m), which is consistent with the enhanced π-conjugation and electron delocalization in the thermally cyclized Ni**L1**-300 framework.

Nickel, coupled with graphene, amorphous carbon or other carbon substrates, is often used for the electrocatalysis of hydrogen evolution reaction (HER)[38-42]. The electrocatalytic

performance of Ni**L1** and Ni**L1**-300 as HER catalysts was carried out by the method of rotating disk electrode in a three-electrode system (details can be seen in ESI). In a 0.5 M H_2SO_4 solution, the Ni**L1** electrode gave a η_{10} of 891 mV, and a Tafel slope of 258 mV/dec (Figure 4). Compared to Ni**L1**, the thermocyclized sample of Ni**L1**-300 exhibits a smaller overpotential of 698 mV at the current density of 10 mA/cm² and a Tafel slope of 158 mV/dec, which is consistent with the enhanced charge transport in Ni**L1**-300. For better catalytic performance, palladium(II) was loaded to form Ni**L1**-300-Pd by soaking the Ni**L1**-300 solid in a CH_3CN solution of $PdCl_2$. PXRD (Figure S10) of the resultant Ni**L1**-300-Pd indicates retention of the crystalline order. Elemental analysis by ICP-OES quantifies the Ni/Pd atomic ratio to be 17.3:1, indicating a small loading of Pd; nevertheless, significantly enhanced HER performance was achieved, with a much smaller overpotential of 383 mV at the current density of 10 mA/cm² and a Tafel slope of 137 mV/dec.

Finally, carbon black was ground with Ni**L1**-300-Pd to enhance the conductivity in order to further improve the HER performance. In 0.5 M H_2SO_4 electrolyte, the Ni**L1**-300-Pd/carbon blend successfully reduced the overpotential down to 293 mV at the current density of 10 mA/cm² and a Tafel slope of 97 mV/dec, thus achieving HER activity comparable with some of the topical nickel/palladium-enabled materials (e.g., the overpotential at 10 mA/cm² and Tafel slope of THAT-Ni single layer: 315 mV, 76 mV/dec; Ni@C_2N: 450 mV, 165 mV/dec; Pd@C2N: 289 mV, 188 mV/dec).[43-47] The thermal treatment of Ni**L1** as well as the metal loading steps can likely be further modulated for potentially better electrocatalytic properties.

ASSOCIATED CONTENT

Supporting Information

General synthetic experimental details, NMR spectra, details of the structure simulation, PXRD, TGA, XPS, SEM images and LSV curves. This material is available free of charge *via* the Internet at http://doi.org/XXXX.

AUTHOR INFORMATION

Corresponding Author

Zhengtao Xu* City University of Hong Kong, 83 Tat Chee Avenue, Kowloon, Hong Kong, P. R. China; ORCID iD: 0000-0002-7408-4951; Phone: 852 34424679; Email: zhengtao@cityu.edu.hk

Jun He* School of Chemical Engineering and Light Industry, Guangdong University of Technology, Guangzhou, 510006, Guangdong, P. R. China; ORCID iD: 0000-0001-7062-4001; Phone: 86 138 2211 8686; Email: junhe@gdut.edu.cn

Notes

The authors declare no competing financial interests.

ACKNOWLEDGMENT

This work was supported by the National Natural Science Foundation of China (21871061, 21901046), Local Innovative and Research Teams Project of Guangdong Pearl River Talents Program (2017BT01Z032) and Science and Technology Planning Project of Guangdong Province (2017A050506051), Science and Technology Program of Guangzhou (201807010026). Z.X. acknowledges a GRF grant from the Research Grants Council of HKSAR (CityU 11306018), and an SRG grant of City University of Hong Kong (Project 7004820).

REFERENCES

1 Y. Diao, J. Hu, S. Cheng, F. Ma, M.-Q. Li, X. Hu, Y. Y. Li, J. He and Z. Xu, Dense Alkyne Arrays of a Zr(IV) Metal-Organic Framework Absorb $Co_2(CO)_8$ for Functionalization, *Inorg. Chem.*, 2020, **59**, 5626-5631.

2 S.-X. Cheng, P. Tieu, W. Gao, J. Hu, W. Feng, J. He, X.-Q. Pan and Z. Xu, Crystallinity after decarboxylation of a metal-carboxylate framework: indestructible porosity for catalysis, *Dalton Trans.*, 2020, Ahead of Print. DOI: https://doi.org/10.1039/D0DT02075C.

3 Y.-L. Hou, M.-Q. Li, S. Cheng, Y. Diao, F. Vilela, Y. He, J. He and Z. Xu, Dramatic improvement of stability by in situ linker cyclization of a metal-organic framework, *Chem. Commun.*, 2018, **54**, 9470-9473.

4 L. S. Xie, G. Skorupskii and M. Dincă, Electrically Conductive Metal-Organic Frameworks, *Chem. Rev.*, 2020, **120**, 1536-8580.

5 P. Thanasekaran, T.-T. Luo, J.-Y. Wu and K.-L. Lu, Giant metal-organic frameworks with bulky scaffolds: from microporous to mesoporous functional materials, *Dalton Trans.*, 2012, **41**, 5437-5453.

6 N. Huang, S. Yuan, H. Drake, X. Yang, J. Pang, J. Qin, J. Li, Y. Zhang, Q. Wang, D. Jiang and H. C. Zhou, Systematic Engineering of Single Substitution in Zirconium Metal-Organic Frameworks toward High-Performance Catalysis, *J. Am. Chem. Soc.*, 2017, **139**, 18590-18597.

7 J.-S. Qin, S. Yuan, L. Zhang, B. Li, D.-Y. Du, N. Huang, W. Guan, H. F. Drake, J. Pang, Y.-Q. Lan, A. Alsalme and H.-C. Zhou, Creating Well-Defined Hexabenzocoronene in Zirconium Metal-Organic Framework by Postsynthetic Annulation, *J. Am. Chem. Soc.*, 2019, **141**, 2054-2060.

8 K. Li, Z. Xu, H. Xu and J. M. Ryan, Semiconductive Coordination Networks from 2,3,6,7,10,11-Hexakis(alkylthio)triphenylenes and Bismuth(III) Halides: Synthesis, Structure-Property Relations, and Solution Processing, *Chem. Mater.*, 2005, **17**, 4426-4437.

9 R. Dong, Z. Zhang, D. C. Tranca, S. Zhou, M. Wang, P. Adler, Z. Liao, F. Liu, Y. Sun, W. Shi, Z. Zhang, E. Zschech, S. C. B. Mannsfeld, C. Felser and X. Feng, A coronene-based semiconducting two-dimensional metal-organic framework with ferromagnetic behavior, *Nat. Commun.*, 2018, **9**, 1-9.

10 J. Cui and Z. Xu, An electroactive porous network from covalent metal-dithiolene links, *Chem. Commun.*, 2014, **50**, 3986-3988.

11 L. Cao, Z. Lin, W. Shi, Z. Wang, C. Zhang, X. Hu, C. Wang and W. Lin, Exciton Migration and Amplified Quenching on Two-Dimensional Metal-Organic Layers, *J. Am. Chem. Soc.*, 2017, **139**, 7020-7029.

12 C. Wang, Z. Xie, K. E. De Krafft and W. Lin, Doping Metal-Organic Frameworks for Water Oxidation, Carbon Dioxide Reduction, and Organic Photocatalysis, *J. Am. Chem. Soc.*, 2011, **133**, 13445-13454.

13 B. Lu, Y. Chen, P. Li, B. Wang, K. Mullen and M. Yin, Stable radical anions generated from a porous perylenediimide metal-organic framework for boosting near-infrared photothermal conversion, *Nat. Commun.*, 2019, **10**, 767.

14 P. Deria, D. A. Gomez-Gualdron, W. Bury, H. T. Schaef, T. C. Wang, P. K. Thallapally, A. A. Sarjeant, R. Q. Snurr, J. T. Hupp and O. K. Farha, Ultraporous, Water Stable, and Breathing Zirconium-Based Metal-Organic Frameworks with ftw Topology, *J. Am. Chem. Soc.*, 2015, **137**, 13183-13190.

15 C. Hua, P. W. Doheny, B. Ding, B. Chan, M. Yu, C. J. Kepert and D. M. D'alessandro, Through-Space Intervalence Charge Transfer as a Mechanism for Charge Delocalization in Metal-Organic Frameworks, *J. Am. Chem. Soc.*, 2018, **140**, 6622-6630.

16 W.-H. Li, W.-H. Deng, G.-E. Wang and G. Xu, Conductive MOFs, *EnergyChem*, 2020, **2**, 100029.

17 N. A. Vermeulen, O. Karagiaridi, A. A. Sarjeant, C. L. Stern, J. T. Hupp, O. K. Farha and J. F. Stoddart, Aromatizing Olefin Metathesis by Ligand Isolation inside a Metal- Organic Framework, *J. Am. Chem. Soc.*, 2013, **135**, 14916-14919.

18 T. C. Wang, W. Bury, D. A. Gomez-Gualdron, N. A. Vermeulen, J. E. Mondloch, P. Deria, K. Zhang, P. Z. Moghadam, A. A. Sarjeant, R. Q. Snurr, J. F. Stoddart, J. T. Hupp and O. K. Farha, Ultrahigh surface area zirconium MOFs and insights into the applicability of the BET theory, *J. Am. Chem. Soc.*, 2015, **137**, 3585-3591.

19 J. S. Qin, S. Yuan, A. Alsalme and H. C. Zhou, Flexible Zirconium MOF as the Crystalline Sponge for Coordinative Alignment of Dicarboxylates, *ACS Appl. Mater. Interfaces*, 2017, **9**, 33408-33412.

20 S. Krause, V. Bon, U. Stoeck, I. Senkovska, D. M. Többens, D. Wallacher and S. Kaskel, A Stimuli-Responsive Zirconium Metal-Organic Framework Based on Supermolecular Design, *Angew. Chem., Int. Ed.*, 2017, **56**, 10676-10680.

21 Y. Zhang, X. Zhang, J. Lyu, K. I. Otake, X. Wang, L. R. Redfern, C. D. Malliakas, Z. Li, T. Islamoglu, B. Wang and O. K. Farha, A Flexible Metal-Organic Framework with 4-Connected Zr_6 Nodes, *J. Am. Chem. Soc.*, 2018, **140**, 11179-11183.

22 J. B. Decoste, G. W. Peterson, H. Jasuja, T. G. Glover, Y.-G. Huang and K. S. Walton, Stability and degradation mechanisms of metal-organic frameworks containing the $Zr_6O_4(OH)_4$ secondary building unit, *J. Mater. Chem. A*, 2013, **1**, 5642-5650.

23 M. C. Lawrence, C. Schneider and M. J. Katz, Determining the structural stability of UiO-67 with respect to time: a solid-state NMR investigation, *Chem. Commun.*, 2016, **52**, 4971-4974.

24 N. Masciocchi, S. Galli, V. Colombo, A. Maspero, G. Palmisano, B. Seyyedi, C. Lamberti and S. Bordiga, Cubic Octanuclear Ni(II) Clusters in Highly Porous Polypyrazolyl-Based Materials, *J. Am. Chem. Soc.*, 2010, **132**, 7902-7904.

25 K. Wang, X. L. Lv, D. Feng, J. Li, S. Chen, J. Sun, L. Song, Y. Xie, J. R. Li and H. C. Zhou, Pyrazolate-Based Porphyrinic Metal-Organic Framework with Extraordinary Base-Resistance, *J. Am. Chem. Soc.*, 2016, **138**, 914-919.

26 X. L. Lv, K. Wang, B. Wang, J. Su, X. Zou, Y. Xie, J. R. Li and H. C. Zhou, A Base-Resistant Metalloporphyrin Metal-Organic Framework for C-H Bond Halogenation, *J. Am. Chem. Soc.*, 2017, **139**, 211-217.

27 N. Huang, K. Wang, H. Drake, P. Cai, J. Pang, J. Li, S. Che, L. Huang, Q. Wang and H. C. Zhou, Tailor-Made Pyrazolide-Based Metal-Organic Frameworks for Selective Catalysis, *J. Am. Chem. Soc.*, 2018, **140**, 6383-6390.

28 L. Mino, V. Colombo, J. G. Vitillo, C. Lamberti, S. Bordiga, E. Gallo, P. Glatzel, A. Maspero and S. Galli, Spectroscopic and adsorptive studies of a thermally robust pyrazolato-based PCP, *Dalton Trans.*, 2012, **41**, 4012-4019.

29 S. Cheng, K. Li, J. Hu, J. He, M. Zeller and Z. Xu, Building Conjugated Donor-Acceptor Cross-Links into Metal-Organic Frameworks for Photo- and Electroactivity, *ACS Appl. Mater. Interfaces*, 2020, **12**, 19201-19209.

30 W. R. Xian, Y. He, Y. Diao, Y. L. Wong, H. Q. Zhou, S. L. Zheng, W. M. Liao, Z. Xu and J. He, A Bumper Crop of Boiling-Water-Stable Metal-Organic Frameworks from Controlled Linker Sulfuration, *Inorg. Chem.*, 2020, **59**, 7097-7102.

31 M. Carboni, Z. Lin, C. W. Abney, T. Zhang and W. Lin, A metal-organic framework containing unusual eight-connected Zr-oxo secondary building units and orthogonal carboxylic acids for ultra-sensitive metal detection, *Chemistry*, 2014, **20**, 14965-14970.

32 V. Colombo, S. Galli, H. J. Choi, G. D. Han, A. Maspero, G. Palmisano, N. Masciocchi and J. R. Long, High thermal and chemical stability in pyrazolate-bridged metal-organic frameworks with exposed metal sites, *Chem. Sci.*, 2011, **2**, 1311-1319.

33 T. He, Z. Huang, S. Yuan, X.-L. Lv, X.-J. Kong, X. Zou, H.-C. Zhou and J.-R. Li, Kinetically Controlled Reticular Assembly of a Chemically Stable Mesoporous Ni(II)-Pyrazolate Metal-Organic Framework, *J. Am. Chem. Soc.*, 2020, **142**, 13491-13499.

34 N. M. Padial, E. Quartapelle Procopio, C. Montoro, E. Lopez, J. E. Oltra, V. Colombo, A. Maspero, N. Masciocchi, S. Galli, I. Senkovska, S. Kaskel, E. Barea and J. A. Navarro, Highly hydrophobic isoreticular porous metal-organic frameworks for the capture of harmful volatile organic compounds, *Angew. Chem. Int. Ed. Engl.*, 2013, **52**, 8290-8294.

35 Y.-Z. Zhang, T. He, X.-J. Kong, Z.-X. Bian, X.-Q. Wu and J.-R. Li, Single-Crystal Synthesis and Structures of Highly Stable Ni8-Pyrazolate-Based Metal–Organic Frameworks, *ACS Mater. Lett.*, 2019, **1**, 20-24.

36 C. Heering, I. Boldog, V. Vasylyeva, J. Sanchiz and C. Janiak, Bifunctional pyrazolate-carboxylate ligands for isoreticular cobalt and zinc MOF-5 analogs with magnetic analysis of $\{Co_4(\mu_4\text{-}O)\}$ node, *CrystEngComm*, 2013, **15**, 9757-9768.

37 T. He, Y. Z. Zhang, H. Wu, X. J. Kong, X. M. Liu, L. H. Xie, Y. Dou and J. R. Li, Functionalized Base-Stable Metal-Organic Frameworks for Selective CO2 Adsorption and Proton Conduction, *Chemphyschem*, 2017, **18**, 3245-3252.

38 L. Ai, T. Tian and J. Jiang, Ultrathin Graphene Layers Encapsulating Nickel Nanoparticles Derived Metal–Organic Frameworks for Highly Efficient Electrocatalytic Hydrogen and Oxygen Evolution Reactions, *ACS Sustainable Chem. Eng.*, 2017, **5**, 4771-4777.

39 M. Chu, L. Wang, X. Li, M. Hou, N. Li, Y. Dong, X. Li, Z. Xie, Y. Lin, W. Cai and C. Zhang, Carbon coated nickel - Nickel oxide composites as a highly efficient catalyst for hydrogen evolution reaction in acid medium, *Electrochim. Acta*, 2018, **264**, 284-291.

40 H. Liu, M. Zhang, T. Ma and Y. Wang, Ni and NiO in situ grown on sulfur and phosphorus co-doped graphene as effective bifunctional catalyst for hydrogen evolution, *J. Electroanal. Chem.*, 2019, **848**, 113306.

41 Y. Xu, W. Tu, B. Zhang, S. Yin, Y. Huang, M. Kraft and R. Xu, Nickel Nanoparticles Encapsulated in Few-Layer Nitrogen-Doped Graphene Derived from Metal-Organic Frameworks as Efficient Bifunctional Electrocatalysts for Overall Water Splitting, *Adv. Mater.*, 2017, **29**, 1605957.

42 L. Yan, P. Dai, Y. Wang, X. Gu, L. Li, L. Cao and X. Zhao, In Situ Synthesis Strategy for Hierarchically Porous Ni2P Polyhedrons from MOFs Templates with Enhanced Electrochemical Properties for Hydrogen Evolution, *ACS Appl. Mater. Interfaces*, 2017, **9**, 11642-11650.

43 J. Mahmood, F. Li, S. M. Jung, M. S. Okyay, I. Ahmad, S. J. Kim, N. Park, H. Y. Jeong and J. B. Baek, An efficient and pH-universal ruthenium-based catalyst for the hydrogen evolution reaction, *Nat. Nanotechnol.*, 2017, **12**, 441-446.

44 R. Dong, Z. Zheng, D. C. Tranca, J. Zhang, N. Chandrasekhar, S. Liu, X. Zhuang, G. Seifert and X. Feng, Immobilizing Molecular Metal Dithiolene-Diamine Complexes on 2D Metal-Organic Frameworks for Electrocatalytic H_2 Production, *Chemistry*, 2017, **23**, 2255-2260.

45 T. Tian, L. Ai and J. Jiang, Metal–organic framework-derived nickel phosphides as efficient electrocatalysts toward sustainable hydrogen generation from water splitting, *RSC Adv.*, 2015, **5**, 10290-10295.

46 V. Veeramani, B. M. Matsagar, Y. Yamauchi, A. Y. Badjah, M. Naushad, M. Habila, S. Wabaidur, Z. A. Alothman, Z.-L. Wang and K. C. W. Wu, Metal organic framework derived nickel phosphide/graphitic carbon hybrid for electrochemical hydrogen generation reaction, *J. Taiwan Inst. Chem. E.*, 2019, **96**, 634-638.

47 M. Nie, H. Sun, D. Lei, S. Kang, J. Liao, P. Guo, Z. Xue and F. Xue, Novel Pd/MOF electrocatalyst for hydrogen evolution reaction, *Mater. Chem. Phys.*, 2020, **254**, 123481.